Journal of the Korean Nuclear Society
Volume 30, Number 6, pp.518~530, December 1998

Chemical Methods Used in Petrological Analysis of Koongarra Uranium Ore Samples in ASSAR Natural Analogue Program

Yong Joon Park, Hyung Ryul Pyo, Ji Young Kim, and Won Ho Kim
Korea Atomic Energy Research Institute
150 Dukjin-dong, Yusong-gu, Taejon 305-353, Korea

(Received October 10, 1997)

Abstract

A natural analogue study has been performed for the Koongarra uranium ore deposit in Australia as an international agreement of the Analogue Studies in the Alligator Rivers Region (ASARR). Rocks obtained from the Koongarra deposit, Northern Territory of Australia, were examined in order to understand uranium migration processes of primary and secondary ore-body in both weathered and unweathered zones. Total alpha activities of rock samples were measured to compare the relative amount of uranium in the sample. Uranium distributions have been investigated by means of both the alpha-autoradiography and the fission track registration technique after irradiation in a flux of thermal neutrons ($\sim 1.0 \times 10^{13}$ n $\cdot$ cm^{-2} $\cdot$ s^{-1}) for 2 minutes. The mineral phases corresponding to the registered alpha-tracks and fission tracks were identified by petrological observation with optical microscope as well as X-ray diffraction and electron microprobe analysis (EPMA). Uranium was found mostly inside of the fracture of the quartzite and its mineral phase was identified as sklodowskite. The mineral phase associated with high uranium concentration was found as illeminite by petrological observation with optical microscope as well as EPMA.

1. Introduction

The importance of geochemistry arises from the requirement to make scientifically sound evaluations of the long-term radiological safety of repositories. Knowledge of the nature and evolution of goechemical and hydrothermal regimes is fundamental to make predictions of the behavior and health impact of radionuclides released from the wastes with timescales of tens to thousands million years. This is important particularly for deep radioactive waste repositories, situated several hundreds of meters below the surface and designed to contain the radioactive waste with the longest half-live radionuclides.

Clearly, long-term predictions of the behavior of natural environment have uncertainty if they are based solely on short-term experiments. In order to reduce this uncertainty, or at least to put it in context with other uncertainties in predictions of

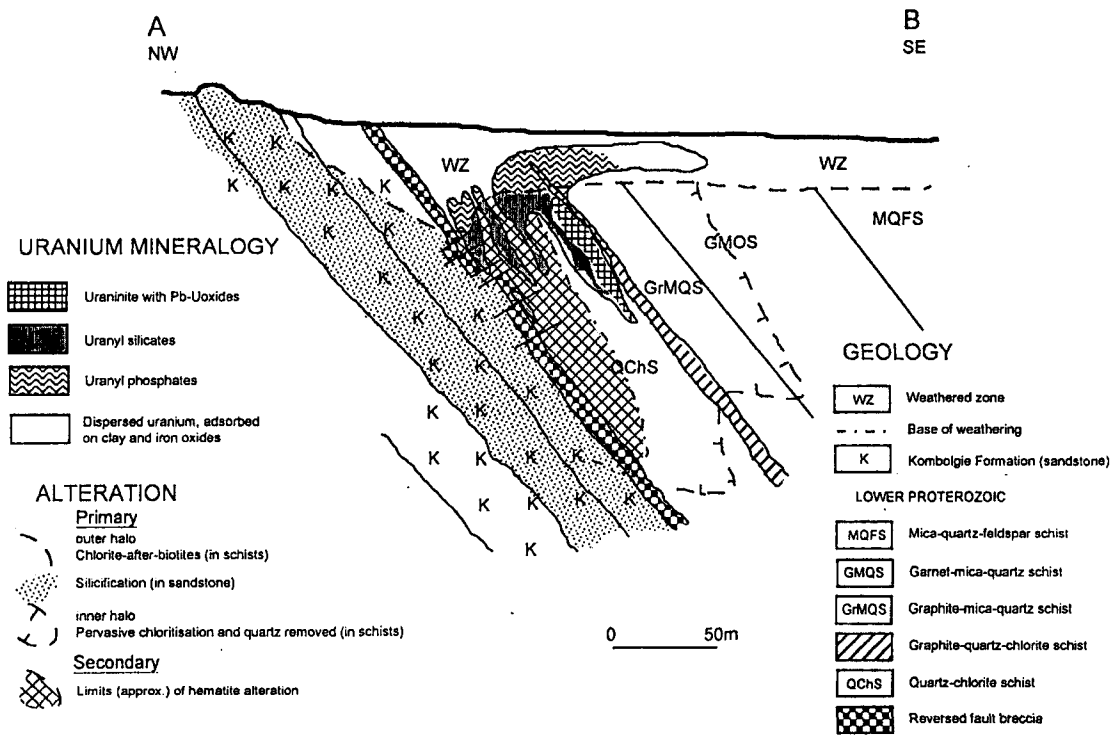

Fig. 1. Simplified Cross-section Through the Koongara No. 1 Ore-boby Showing the Geology and the Distribution of Uranium Minerals and Alteration(After Snelling, 1990)

the future behavior of the natural environment, it is vital to tie to well-recognized and long-term natural processes of a broadly equivalent nature. Such as parallels are known as natural analogues [1]. Since uranium deposits are the result of the alteration, transportation, dispersion, migration and concentration of uranium in the Earth' s near surface over geological periods of time, it has been used as an analogue to the possible long-term behavior of uranium in direct disposal of spent nuclear fuels when exposed to similar relevant conditions.

Up to now, various "natural analogue" studies have been carried out on ore-bodies as listed below:

Maquarin area in Jordan: Natural analogue of high pH cement pore water [2]

Oklo area in Gabon: Migration of fission products into microminerals of Oklo Natural Reactors [3]

Cigar Lake area in Canada: Characterization of the surfaces of the uranium minerals [4]

Koongarra area in Australia: Weathering and its effects on uranium redistribution [5]

El Berrocal area in Spain: U/Th series disequilibrium study [6]

Tono area in Japan: Uranium series disequilibrium study [7, 8]

Among those studies a natural analogue study for the Koongarra uranium ore deposit in Australia has been carried out by Alligator Rivers Analogue Project (ARAP) through an international research program sponsored by the OECD Nuclear Energy Agency (NEA) since 1987. Six organizations including the Australian Nuclear Science and Technology Organization (ANSTO), the Japan

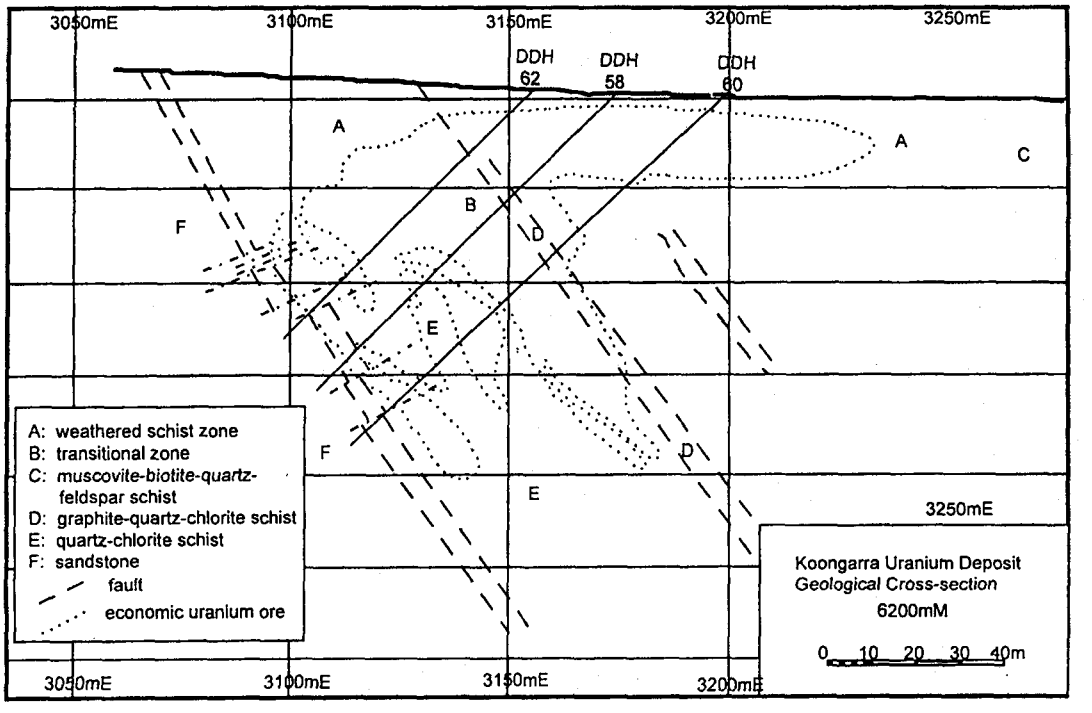

Fig. 2. Koongarra Cross-section Showing Geology, Drill Holes and Outline of Economic Mineralization Grades.

Atomic Energy Research Institute (JAERI), the Power Reactor and Nuclear Fuel Development Corporation of Japan (PNC), the Swedish Nuclear Power Inspectorate (SKI), the UK Department of the Environment (UKDoE), and the US Nuclear Regulatory Commission (USNRC) were participated in the program. In 1996, an extended program was reached by a number of agencies concerning with radioactive waste disposal, to set up the Analogue Studies in the Alligator Rivers Region (ASARR). The Korea Atomic Energy Research Institute (KAERI) participated in this international project with other following organizations: JAERI and USNRC.

The Koongarra uranium deposit is located at 225 km east of the city of Darwin and 25 km south of the town of Jabiru at latitude 12°52′S, longitude 123°50′E in the Northern Territory of Australia, in the area known as the Alligator River Region. It is one of four major uranium deposits discovered in the region. Geologic, geochemical and hydrogeological informations were described in ARAP report [9].

Even though there are two ore-bodies in the Koongarra uranium deposit, most attention has been focussed on the No. 1 ore-body, the shallower of the two. Within the objectives of the natural analogue studies the Koongarra No. 1 ore-body has proven to be most suitable for validation of models for radionuclide transport. The simplified cross section of the Koongarra No. 1 ore-body is shown in Fig. 1. In the Koongarra No. 1 ore-body, there are well-defined zones of primary, weathered primary and dispersion fan ore. There has been a weathering process of the primary ore to the weathered primary ore, and

Table 1. Drill Record for Uranium Rock Samples Obtained from DDH60, DDH58 and DDH62 Drill Holes

Core	Sample No.	from	to	U_3O_8	Geological Log
DDH 60	G2760	200.0	205.0	62.00	Quartz chlorite schist with weak to medium hematitic alteration. Locally, visible pitchblende from 195.5′ to 196.5′ and from 195.5′ to 200.0′, occurs as thin up to 1/10″ stringers mainly parallel to schistosity but with some cross cutting, accompanied by strong hematitic alteration, and traces of galena. There is shearing from 196.0′ to 197.0′, and strong shearing from 200.0′ to 203.0′ in quartz chlorite schist with hematitic alteration
DDH 58	G2676	31.0	35.0	2.48	Fragments of quartz with grey clay. Heavy core loss.
	G2678	40.0	45.0	3.20	Slightly less weathered, dominantly red stained, quartz mica schist. Some lighter streaks. Some quartz stringers up to 1″ thick.
	G2685	75.0	80.0	6.00	ditto
	G2688	91.0	95.0	2.76	Abrupt change to much less decomposed rock. Very well defined schistosity. Quartz chlorite muscovite schist with garnets. Some thin up to 1/4″ quartz stringers. Obvious hematite staining parallel to schistosity.
	G2691	105.0	113.8	9.91	Less weathered quartz chlorite schist with minor muscovite. Well defined schistosity.
	G2695	121.3	126.3	17.20	Black graphitic schist with abundant fine pyrite, minor galena and probably pitchblende. Strong shearing and cross fracturing.
	G2696	126.3	129.5	186.00	Quartz chlorite schist with well defined schistosity. Zones of blue black pitchblende and minor galena associated with strong hematite alteration in quartz form. Yellow secondary uranium minerals in last six inches.
	G2701	141.5	143.1	72.60	Fractured quartzite with yellow secondary uranium minerals in the fractures.
	G2704	155.0	160.0	100.00	Fractured, quartzite banded, quartz chlorite schist with pitchblende and abundant secondary uranium minerals in the fractures.

Table 1. Drill Record for Uranium Rock Samples Obtained from DDH60, DDH58 and DDH62 Drill Holes

Core	Sample No.	from	to	U_3O_8	Geological Log
DDH 62	G2803	50.0	55.0	4.32	Dark red hematitic, decomposed quartz chlorite? schist. Schistosity well defined in places. Lignite, goethite and manganese coatings along schistosity planes and fractures.
	G2806	65.0	70.0	25.40	Red, hematitic, decomposed quartz chlorite? schist. Yellow and green uranophosphates(saleeite) present over whole 5.0′.
	G2810	85.0	90.0	7.96	Transition zone from decomposed hematitic schist to less weathered reddish-grey quartz chlorite? schist. Abundant yellow-green urano-phosphate mineral along schistosity planes. Green platy urano-phosphate minerals very abundant at 88.2′. Numerous quartz fragments up to 0.5″ at 87.7′ (ex vein material).
	G2811	90.0	95.0	4.24	Partially weathered quartz chlorite schist, well defined shistosity. Yellow-green uranophosphate minerals common in schistosity planes. Fairly broken.

then the dispersal of uranium from the weathered primary ore to the dispersion fan ore, which provide the two potential analogues. The ore-body contains 0.44% U_3O_8 and is 450 m long and 100 m deep. The cross-section showing geology and drill holes for the 14 samples obtained are shown in Fig. 2. The Drill records for the rock samples obtained from DDH60, DDH58 and DDH62 drill hole are tabulated in Table 1.

2. Experimental

Samples were treated in two different ways, as powders and thin sections. The powdered samples were subjected to X-ray powder diffractometry (XPD), chemical analysis, and alpha spectroscopy. Polished petrological thin sections were prepared from samples and checked initially by optical microscopy (OM), alpha-autoradiography and fission tracking method as followed by scanning electron microscopy (SEM) and electron microprobe analysis (EPMA).

The XPD patterns were recorded on a Siemens model D5000 diffractometer, using a CuKα radiation (λ=1.5406Å). The 2θ scan rate was 2.4° min^{-1}, the current 30 mA and the voltage 40 kV. The diffraction patterns were normally taken in the range of $10° \leq 2\theta \leq 50°$.

Uranium distributions have been investigated by means of both the alpha-autoradiography and the fission track registration technique after irradiation in a flux of thermal neutrons($\sim 1.0 \times 10^{13}$ n · cm^{-2} · s^{-1}) for 2 minutes. Lexan polycarbonate plastic film was used as the solid state nuclear fission track detector. The detector was directly contacted with the polished surface of a thin section for exposure

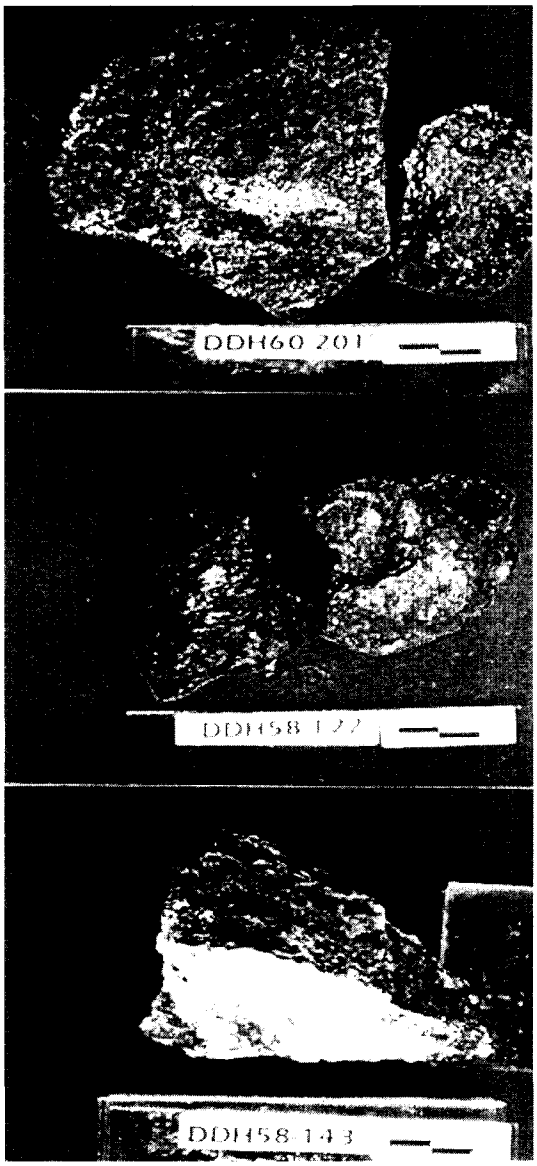

Fig. 3. Photos of the Three Different Rocks Formed in Koongarra Site. a) Chlorite Schist (DDH60-201) b) Graphite Schist (DDH58-122) c) Quartzite (DDH58-143)

times of 14 days. After exposure, the detectors were etched in NaOH solution. The optimum etching conditions of the Lexan plastic was found to be 60 ℃, 5 hours, and 6.25 M NaOH solution for alpha tracks and 70 ℃, 10 minutes, and 6.25 M NaOH solution for fission tracks.

The mineral faces corresponding to the registered alpha-tracks and fission tracks were identified by petrological observation with OM. Wavelength dispersive spectrometry (WDS) was used for the quantitative analysis of selected elements while energy dispersive spectrometry (EDS) was used for full spectral checks. Spot analyses were conducted on areas of high alpha activity.

3. Results and Discussion

3.1. Sample Description

The 14 samples obtained from the Koongarra uranium ore deposit are divided into two groups: one is from primary ore-body and the others from secondary ore-body. The typical 3 rock series composed in these samples were chlorite schist, quarzite, and graphite schist as shown in Fig. 3. Most of samples obtained from the primary ore-body were dark grey chlorite schists. Samples of DDH58-143 and DDH58-160 are pale pink-colored quarzites, while DDH58-122 is dark-colored graphite schist. The main mineral constituents of the host schist are quartz, chlorite and muscovite. Within the primary ore zone the nature of the chlorite is mainly magnesium-rich. Some samples of DDH62-88, DDH62-94, DDH58-127 and DDH60-201 are from the vicinity of the fracture zone.

Rock samples from the weathered zone above the primary ore-body are reddish brown, soft and brittle. Samples of DDH62-51, DDH62-69, DDH58-30, and DDH58-43 are strongly weathered while samples of DDH58-76 and DDH58-106 are under the weathering procedure and shows well-developed or distorted schistosity. Detailed results of bare-eye observation and optical microscopic observation of these samples were tabulated in Table 2.

Table 2. Observation and Crude Description for Uranium Rock Samples Obtained from DDH60, DDH58 and DDH62 Drill Holes

Core	Sample No.	Depth(ft)	U_3O_8	Observation
DDH 60	DDH60-201 G2760	201.0	62.00	dark gray, chlorite schist yellow minerals stained fracture perpendicular to the schistosity
DDH 58	DDH58-30 G2676	30.0	2.48	strongly weathered, reddish brown, mica schist micaeous and schistose soft and fragile
	DDH58-43 G2678	43.0	3.20	purple red, strongly weathered schistose, soft and fragile, mica schist
	DDH58-76 G2685	76.0	6.00	purple red, deeper than DDH58-43 strongly weathered, schistose, soft and fragile mica schist
	DDH58-92 G2688	92.0	2.76	well defined schistose structure, quartz mica schist soft and weathered fracture surface
	DDH58-106 G2691	106.0	9.91	grey, slightly weathered chlorite schist fracture crosscuts well defined schistosity reddish brown mineral band in the fracture
	DDH58-122 G2695	122.0	17.20	fresh and fractured particles, graphite schist (dark gray) dark blue green seam of 0.5mm thickness (probably not pitchblende) reddish grain on schist
	DDH58-122 G2695	122.0	17.20	grey, slightly weathered chlorite schist fracture crosscuts well defined schistosity reddish brown mineral band in the fracture
	DDH58-127 G2696	127.6	186.00	chlorite schist, reddish schistosity paralleled to schistosity yellow mineral dark blots around and parallel to schistosity red seam of mineral
	DDH58-143 G2701	143.0	72.60	quartzite, pale pink on surface yellow mineral seam of width less than 0.1mm red brown mineral and yellow mineral on surface
	DDH58-160 G2704	160.0	100.00	quartzite, pale pink yellow mineral on fracture surface of width less than 0.1mm - euhedral rectangular plate shape
DDH 62	DDH62-51 G2803	51.0	4.32	completely weathered, pale reddish schistose (well defined)
	DDH62-69 G2806	69.0	25.40	similar to DDH62-51, pale reddish completely weathered, soft, fragile, and loose relatively fresh, fine grained mica schist, well defined schistosity black mineral in the fracture
	DDH62-88 G2810	88.6	7.96	chlorite schist yellow mineral on fracture surface grain boundary was not clear
	DDH62-94 G2811	94.0	4.24	Chlorite schist yellow mineral on fracture surface

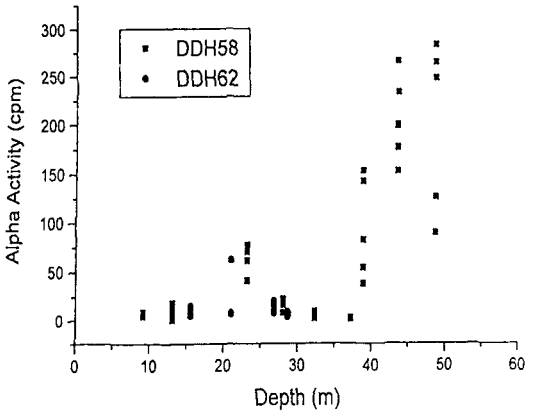

Fig. 4. Variation in Alpha Activities with Depth for DDH58 and DDH60

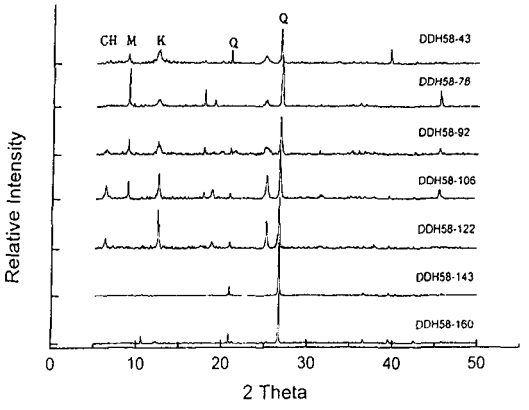

Fig. 5. X-ray Diffractograms of a Suite of the DDH58

3.2. Total alpha activity

Total alpha activities of thin section samples of DDH58 and DDH62 holes were measured to compare the relative content of the uranium in the sample. Although only one sample were from the DDH60, its total alpha activity was measured for the simple comparison with other samples

The plot of the total alpha activities of samples against the sampling depth in DDH58 and 62 holes was shown in Fig. 4. This graph showed a small peak at the depth of around 24 m and a big peak after the depth of 40 m, which are corresponding to the tongue-shaped secondary ore-body and the primary ore-body, respectively. The results can be explained by the comparison with the cross-section view of the Koongarra uranium deposit. From the alpha activity value for the sample obtained in the depth of 61 m in DDH60 hole, it can be concluded that this area is the primary ore-body.

3.3. X-ray diffraction study

Some samples showed yellow or red stains on their surface or certain area. In that case, the specific area was scratched out from the interesting point and collected for the X-ray powder diffraction study. The samples of yellow stain were named by adding 'y' at the end of the sample code (DDH58-127y, DDH58-143y, DDH58-160y, and DDH62-88y), while the samples of red stain were named with 'r' (DDH58-127r).

Changes in mineral compositions with depth can be seen from the X-ray diffractograms of a suite of the DDH58 core hole as shown in Fig. 5. One should note that the distance scale given is not a depth scale but is the distance along the core from the surface. As shown in Fig. 5, chlorite was found in the deep unweathered zone, while mica and kaolinite were observed with decrease in depth. The mica and kaolinite components decrease with increase in depth while the chlorite component increases, except for the DDH58-143 and DDH58-160 samples. This indicates that the mica and kaolinite can be the weathering products for the chlorite. Since the DDH58-143 and DDH58-160 samples are located in the quarzite zone, X-ray pattern of chlorite was not observed but that of quartz.

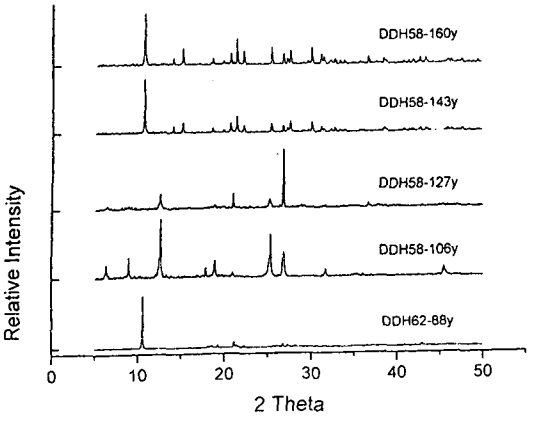

Fig. 6. X-ray Diffractograms of Yellow Powder Grabbed from Rock Samples

The diffraction patterns for the yellow stain on the surface of the rocks (DDH58-127y, DDH58-143y, DDH58-160y, and DDH62-88y) were shown in Fig. 6. As expected from the color of these samples, the samples of DDH58-160y, DDH58-143y and DDH62-88y showed the pattern of sklodowskite (JCPDS file 29-0875) while DDH58-127y and DDH58-106y showed only chlorite, mica, and kaolinite. Sklodowskite, the uranium mineral containing magnesium, were found mostly inside of the fracture of quartzite in DDH58-143 and DDH58-143. However, for the sample of DDH62-88, it exists evenly on the surface of rock sample.

3.4. Alpha Track and Fission Track

Alpha tracking method and fission tracking method by neutron irradiation have been established for the determination of uranium distribution on the thin-section samples. Uranium distribution can be identified by the scars on the plastic plate. The scars on plastic caused either by alpha particles or nuclear fission products produced after neutron irradiation can be easily observed by optical microscope after the etching procedure.

In alpha tracking method, the longer the Lexan plastic is contacted with thin section samples, the more the alpha tracts are observed. Experimentally, the 15 days of contact period resulted that only some tracks were observed in the area of high concentration of uranium for the sample, for example, DDH58-143, DDH62-88 and DDH58-160. However, rare tracts were found for the rest of samples. The alpha tracts in the cleavage area of quartzite for DDH58-143 were shown in Fig. 7. Increasing the contact period to 30 days did not improve the density of the alpha tracks tremendously for the samples containing low uranium content. It is expected that the use of a fission tracking method instead can be more sensitive method with a short irradiation time for those samples with low uranium concentration than an alpha tracking method.

For the fission track registration technique, Lexan plastics is attached with thin-section samples and irradiated with a flux of thermal neutrons ($\sim 1.0 \times 10^{13}$ n $\cdot$ cm^{-2} $\cdot$ s^{-1}) for 2 minutes and then etched to develop the tracks of fission fragment of neutron-induced fissions of atoms on the surface of the plastic detector. One of the advantages of this method compared with the alpha track can definitely be a short measurement time. Therefore, this method is very powerful for the samples of low concentration of uranium, which may take more than a month to have enough sensitivity when using alpha track method.

Low magnification microscopic photographs of thin-section with (1) and without polarizing filters (2) and photographs of Lexan plastic (3) for the DDH58-143 are shown in Fig. 8. Clear grain boundaries can be easily identified with two polarizing filters. Therefore, the relation between mineral information and the uranium distribution can be obtained by comparing the thin-section with the corresponding plastic detector. Fig. 8(c)

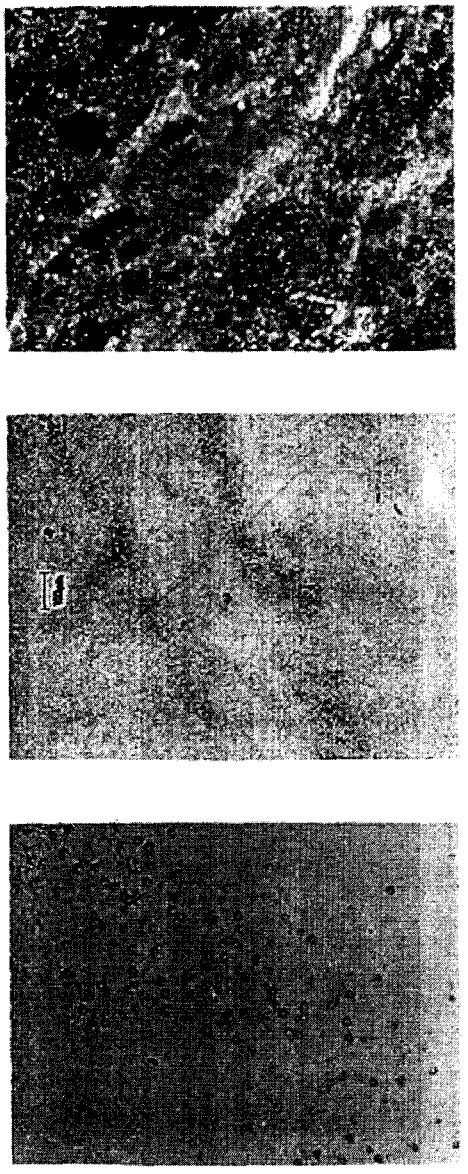

Fig. 7. Symmetrical Feature of Uranium Distribution in the Fracture Area of DDH58-143 Sample. (a) Photograph of the Surface in Thin Section, (b) Uranium Distribution Identified by Alpha Tracks in Lexan Plate, and (c) the Same Photograph of Enlarged (b)(× 200)

showed fission tracks of very low concentration of uranium present in the micro-fracture of quartzite,

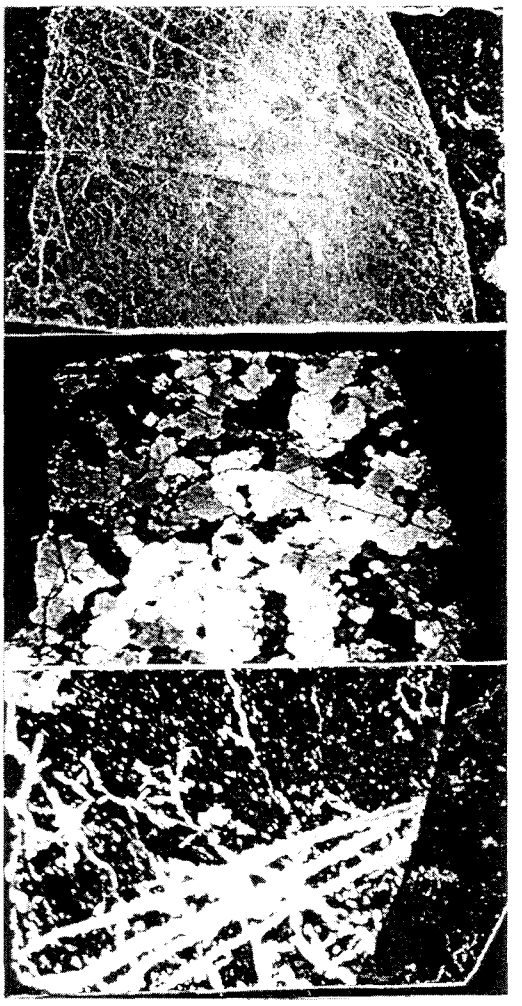

Fig. 8. Symmetrical Feature of Uranium Distribution in the Fracture Area and Grain Boundary of DDH58-143 Sample. (a) Photograph of the Surface in Thin Section(open), (b) of the Same Thin Section(cross), and (c) Uranium Distribution Identified by Fission Tracks in Lexan Plate

which may not be able to be identified by polarized microphotograph (Fig. 8(b)).

Uranium distribution is shown in Fig. 9. Particles of relatively large grain boundary shown at upper left corner of Fig. 9(b) indicated quartz which did not give fission track in Fig. 9(c).

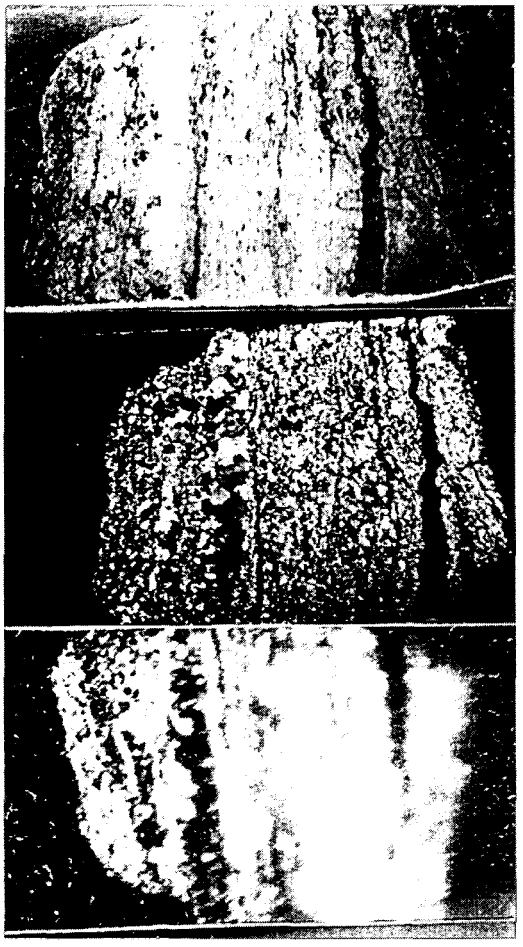

Fig. 9. Symmetrical Feature of Uranium Distribution in the Fracture Area and Grain Boundary of DDH62-69 Sample. (a) Photograph of the Surface in Thin Section(open), (b) of the Same Thin Section(cross), and (c) Uranium Distribution Identified by Fission Tracks in Lexan Plate

3.5. Thin-section Analysis

The nature and distribution of the host rock minerals at Koongarra have been discussed in ARAP reports [3]. Examining the thin sections of the samples from the Koongarra uranium deposit revealed that they contain mostly mica schists, chlorite schists, graphite schists, and quartzite. The texture of most rock particles structurally showed parallel schistosity, typical characteristics of the schists. Porphyroblastic texture was also found from some of the rock samples, which indicate supposedly mafic mineral by means of the weathering mechanism. Some samples were found to be weathered seriously and were composed of weathered or altered secondary minerals. Development of colloidal phase texture was also observed in some samples. The main mineral constituents of the host schists are quartz, chlorite, muscovite, biotite and clay minerals. Iron oxy-hydroxide, rutile, zircon, illemite, and sklodowskite were found as minor phases.

Sklodowskite is the magnesium containing uranium silicate mineral ($Mg(UO_2)_2(SiO_3OH)_2\cdots 5H_2O$), found mostly inside of the fracture of quartzite in DDH58-143 and DDH58-143. This mineral is yellow with eyes, yellowish green with rock microscope and shows parallel extiction with strong birefringence properties. The size of the sklodowskite particle is too small to observe the detailed optical characteristics.

The microscopic observation of thin sections and alpha or fission tracks with optical microscope as well as EPMA was performed in order to find if there are any minerals affecting the uranium distribution or uranium fixation. Among the many mineral phases found in the rock samples, a titanium containing mimeral, ellmenite, was found in the area assocated with high uranium concentration. Microscopic photo of illmenite in the thin section of DDH58-76 sample is shown in Fig. 10, in which brighter area on the upper right corner indicated resin of the thin section and illmenite is shown with white arrows. A tiny particle of iron oxy-hydroxide in the rock sample were also observed by optical microscope. This particle of circular or oval shape showed irregular

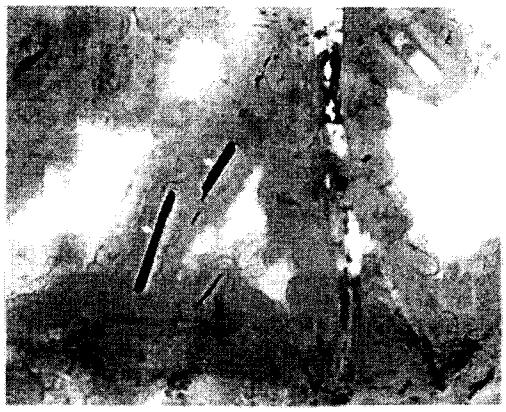

Fig. 10. Microscopic Photo of the Thin Section of DDH58-76 Sample. Illmenite is Shown with the Arrow

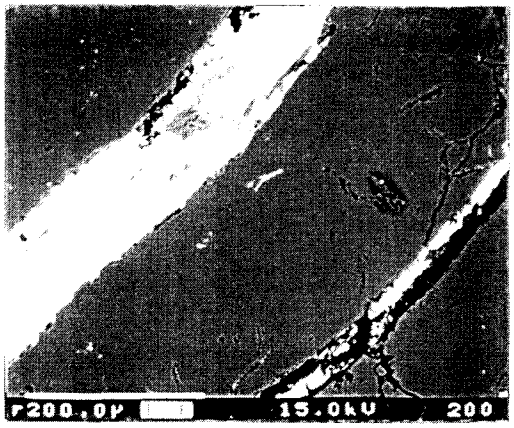

Fig. 11. Backscattered Électron Image of Quartzite. Layers of Uranium Containing Mineral are Shown as Light Tone

Table 3. Chemical Compositions of Sklodowskite (%w/w)

	samples : DDH58-143			
SiO_2	12.588	11.565	12.547	12.645
Al_2O_3	0.076	0.038	0.036	0.236
MgO	4.283	4.553	4.540	4.595
U_2O_6	68.298	69.876	69.183	68.534
Total	85.785	86.032	83.306	86.010

Table 4. Chemical Compositions of Kaolinite (%w/w)

samples	DDH58-30a3	DDH58-75d	DDH58-43a
SiO_2	33.572	35.052	46.125
TiO_2	3.461	7.940	0.150
Al_2O_3	26.208	23.914	32.914
Fe_2O_3	7.826	4.305	1.261
MnO	0.040	0.000	0.000
MgO	0.136	1.913	0.773
CaO	0.018	0.056	0.042
total	72.280	74.273	83.224

Table 5. Chemical Compositions of Muscovite (%w/w)

samples	DDH58-30a1	DDH58-43a1	DDH58-75d
SiO_2	46.692	46.692	45.888
TiO_2	0.008	0.000	0.632
Al_2O_3	34.350	35.546	34.559
Fe_2O_3	0.652	1.355	1.424
MnO	0.014	0.012	0.058
MgO	0.773	0.406	0.686
CaO	0.071	0.011	0.000
Na_2O	0.028	0.058	0.483
K_2O	8.540	9.474	10.279
total	91.092	93.554	94.009

shape of grain boundary. However, this mineral showed patterns of regular stripes and were being developed in close relation with clay minerals.

As shown in Table 3 to 5, the EPMA results of sklodowskite, muscovite and kaolinite provided the confirmation of their mineralogical identification obtained previously by X-ray diffraction patterns. The backscattered electron image of uranium mineral present in the fracture of the quartzite were shown in Fig. 11.

4. Conclusions

The plot of the total alpha activities of samples against the sampling depth in DDH58 showed a small peak at the depth of around 24 m and a big peak after the depth of 40 m, which are corresponding to the tongue-shaped secondary ore-body and the primary ore-body, respectively.

Uranium distributions have been investigated by means of both the alpha-autoradiography and the fission track registration technique after irradiation in a flux of thermal neutrons ($\sim 1.0 \times 10^{13} n \cdot cm^{-2} \cdot s^{-1}$) for 2 minutes. Uranium was found mostly inside of the fracture of the quartzite and its mineral phase was identified as sklodowskite. It can be obtained from this result that the uranium distribution was controlled primarily by crevice compared to the grain boundary or schistosity.

The microscopic studies of mineral phases corresponding to the registered alpha-tracks and fission tracks revealed that illeminite was associated with high uranium concentration by petrological observation with optical microscope as well as EPMA.

References

1. N. A. Chapman, The Pocos de Caldas Project: Natural Analogues of Processes in a Radioactive Waste Repository, Elsevier, New York (1993).
2. Proceedings of the Fourth International Conference on the Chemistry and Migration Behavior of Actinides and Fission Prodects In the Geosphere, Charleston, SC USA, p. 639-644 (1994).
3. H. Hidaka, K. Takahashi and P. Holliger, Radiochimica Acta, **66/67**, 463-468 (1994).
4. S. Sunder, J. J. Cramer adn N. H. Miller, Radiochimica Acta, **74**, 303 (1994).
5. T. Murakami, "Alligator Rivers Anlaogue Project Final Report: wethering and its effects on uranium redistribution" vol. 9 (1992).
6. M. Ivanovich, A. Hernandez Benitez, A. V. Chambers and S. E. Hasler, Radiochimica Acta, **66/67**, 485 (1994).
7. H. Yoshida, K. Kodama and K. Ota, Radiochimica Acta, **66/67**, 505 (1994).
8. T. Nohara, Y. Ochiai, T. Seo and H. Yoshida, Radiochimica Acta, **58/59**, 409 (1992).
9. A. A. Snelling, "Alligator Rivers Anlaogue Project Final Report: geologic setting" vol. 2, p. 4-22 (1992).